Endoscopes and Robots for Tight Surgical Spaces: Use of Precurved Elastic Elements to Enhance Curvature

Andria A. Remirez and Robert J. Webster III

Vanderbilt University, Nashville, TN, USA

ABSTRACT

Many applications in medicine require flexible surgical manipulators and endoscopes capable of reaching tight curvatures. The maximum curvature these devices can achieve is often restricted either by a strain limit, or by a maximum actuation force that the device's components can tolerate without risking mechanical failure. In this paper we propose the use of precurvature to "bias" the workspace of the device in one direction. Combined with axial shaft rotation, biasing increases the size of the device's workspace, enabling it to reach tighter curvatures than a comparable device without biasing can achieve, while still being able to fully straighten. To illustrate this effect, we describe several example prototype devices which use flexible nitinol strips that can be pushed and pulled to generate bending. We provide a statics model that relates the manipulator curvature to actuation force, and validate it experimentally.

Keywords: surgical robots, continuum robots, endoscopes

1. INTRODUCTION

Continuously flexible robots that undergo large deflection are known as "continuum robots". They comprise a large and growing subfield of robotics research. They are frequently applied in surgical applications, because they can reach through small openings and maneuver around obstacles in the body, and because their passive compliance makes them safer than traditional rigid-link robots.[1–3] Flexible endoscopes are one widely known continuum surgical device, and may be robotic or manually actuated.

Continuum robots bend via controlled deformation of an elastic element within the manipulator. A variety of different continuum robot designs have been developed, using different types of elastic elements to provide structural support and transmit actuation forces from a variety of actuators.[3] Tendon-actuated designs, such as those described in [4–7], are some of the most widely used, and are most similar to traditional flexible endoscopes. A tendon-actuated continuum robot typically consists of an elastic structure with tendons attached at the distal tip. The tendons are offset from the central axis of the manipulator, so that when one of the tendons is pulled, it exerts a moment on the tip of the manipulator, causing the flexible backbone to bend. If the robot is experiencing no external loads, it will typically bend into a constant curvature configuration in response to this moment. Under general external loading, the tendons will also exert distributed forces along their lengths, causing the shape to be non-circular.[5] Other continuum robots use multiple flexible rods or tubes instead of tendons, which can transmit forces in two directions (push and pull) rather than one (pull only) to produce bending in a similar way.[8,9] This multi-backbone design has been proposed for surgical procedures including minimally invasive surgery of the throat. Another way to construct a continuum robot is by nesting several precurved elastic tubes inside one another. When the tubes are rotated and translated at their back ends, they bend and twist one another, producing a tentacle-like motion.[10,11] With its needle-size diameter, this type of manipulator has been developed primarily for applications where small size is critical, such as transnasal brain surgery[12] and transurethral prostate surgery.[13] One noteworthy feature of this design is its use of precurved elastic elements.

In this paper, we seek to combine the push-pull concept of [8, 9], with the precurvature concept of [10, 11]. We also propose the use of flat elastic strips in place of round rods for push-pull actuation. These provide high

Further author information: (Send correspondence to A.A.R.)
A.A.R.: E-mail: andria.a.remirez@vanderbilt.edu
R.J.W.: E-mail: robert.webster@vanderbilt.edu

out of plane stiffness, and assuming axial rotation of the device is possible, do not sacrifice workspace. The end result is a new approach for effectively enhancing the achievable curvature of a continuum manipulator, so that it can reach around tighter anatomical corners in the human body, while still being able to fully straighten. The basic concept of adding precurvature, described in Section 2, can be applied to a variety of continuum devices, including those actuated by tendons or push-pull rods.

2. CONCEPT AND CLINICAL MOTIVATION

The maximum curvature a continuum robot can achieve often depends on either material strain limits or actuation forces. To mitigate strain damage, materials with high strain limits are often used. Perhaps the most widely used material is superelastic nitinol, a nickel-titanium alloy with an effective strain limit before plastic deformation that can be as high as 11%.[14] Given this high strain limit, manipulators made with nitinol often fail in some other way before plastic deformation begins. For example, this failure may occur when a glue bond breaks, when a tendon snaps, or when one of the elements begins to buckle.[9] Ensuring that the actuation forces of the manipulator do not exceed some upper limit can prevent most of these failure modes.

With the exception of concentric tube robots, nearly all continuum robots and flexible endoscopes are straight when no actuation forces are applied. In this paper we discuss the idea of precurving the elastic elements in the manipulator, such that the unactuated shape is curved. This has the effect of reducing the material strain in the manipulator when it is actuated to a high curvature pose, and thereby reduces the actuation forces required to achieve that curved pose. The result is a workspace that is "biased" in one direction, as shown in Figure 1, which is capable of achieving tighter curvatures than a non-precurved robot of otherwise the same design. Axial rotation at the base of the manipulator enables the full tip-position workspace, such that the precurved manipulator can reach a larger volume overall.

Medical examples for which higher curvature devices could be useful include retroflexed endoscopy and hip implant revision surgeries. In colonoscopy, which is used as a primary screening tool for colon cancer, the physician uses an endoscope to search the colon for lesions. "Retroflexion" refers to the bending of the endoscope tip to an angle of 180° or more, as illustrated in Figure 2 (a). Retroflexion enables the physician to see features which are not readily visible in the forward view of the endoscope, such as lesions which lie behind folds in the mucosa or near the anal sphincter, and has been shown in a some studies to improve the lesion detection rate.[15,16] In the area of orthopedics, a technique for robotic minimally invasive hip revision surgery has recently been described by Kutzer et al.[6] It involves passing a flexible robot through the screw holes in the acetabular component of the implant to clean out osteolytic bone lesions, as illustrated in Figure 2 (b). Maximizing the curvature of the robot is valuable in this application to more easily clean out regions near the robot's point of entry into the lesion.

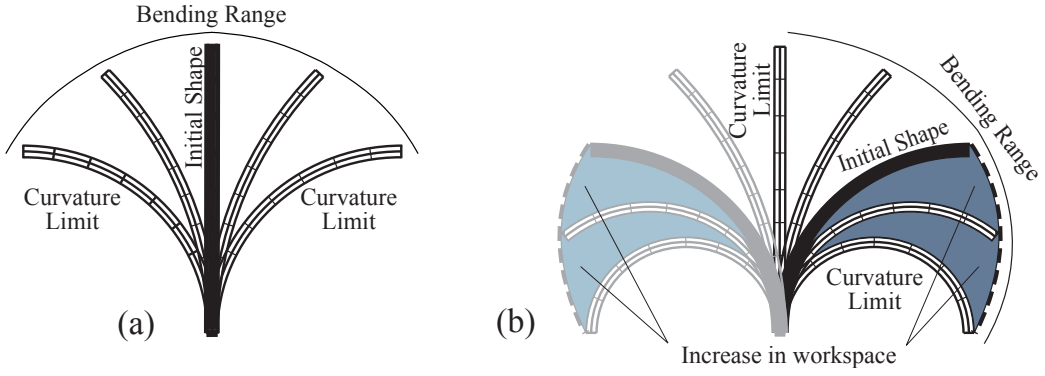

Figure 1: Illustration of the bending ranges of (a) a traditional straight continuum robot and (b) a precurved continuum robot, with their curvature limits defined either by strain limit or by maximum allowable actuation force. The precurved robot is capable of achieving a tighter curvature, and has a larger workspace when axial rotation is allowed.

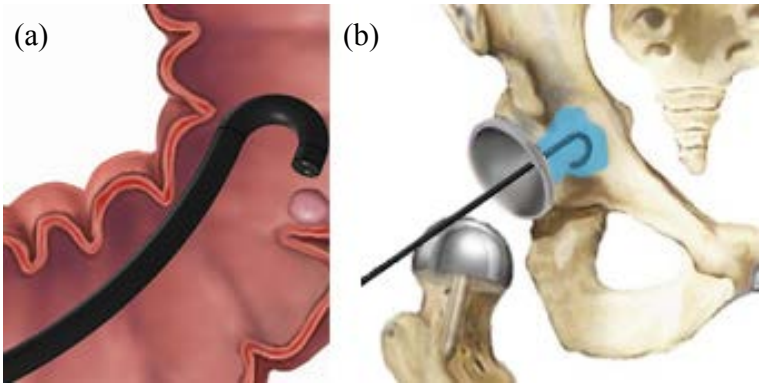

Figure 2: Illustration of how a high-curvature robot could be useful in two specific clinical procedures. (a) shows a colonoscope in retroflexion to find hidden polyps, and (b) shows a curved tool being used to access osteolytic lesions behind the acetabular implant component in hip revision surgery.

3. PROTOTYPE DESIGN

For proof of concept on the use of precurvature to enhance maximum curvature, we constructed a set of three prototypes with different precurvatures. The prototypes, shown in Figure 3, use superelastic nitinol strips as push-pull actuation elements. Each is 7.8 mm in diameter and approximately 40 mm long, with additional dimensions illustrated in Figure 4, and reported in Table 1. The calibrated dimensions in the table refer to values which were experimentally fit to our kinematic model, as described in Section 5.

Each prototype includes a primary backbone strip (labeled "Strip 0" in Figure 4) with spacer discs attached along its length with J-B Weld epoxy. Each prototype also has two additional strips that pass through the spacer discs and transmit actuation forces to the tip of the device. The spacer discs are laser cut from PTFE-filled Delrin acetal resin, selected for low friction. Spacer discs are positioned along the backbone with a spacing of 10 mm. The final disc, located at the tip of the manipulator, is not actually affixed to the central strip; instead the central strip is free to slide in its slot in the tip disc, while the two actuation strips are attached to the tip disc with J-B Weld epoxy. The primary purpose for allowing the central strip to slide at the tip disc is to allow for certain simplifying assumptions in the statics modeling, which are explained in Section 4. To further reduce friction, the actuation strips were coated in a PTFE-based dry lubricant (Duraglide, MicroCare Medical, USA).

To shape-set circular precurvatures into the strips, we used the electrical shape setting method described in [17]. This method involves constraining the strip in the desired shape using a wooden jig and running a large

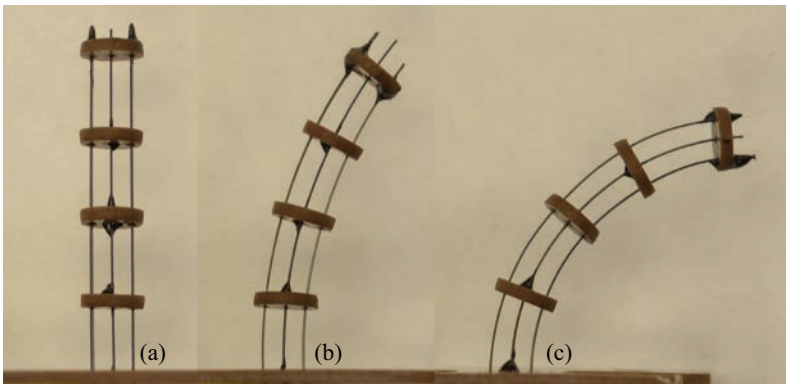

Figure 3: Set of prototype manipulators, with intended precurvature radius values of (a) $\rho_0^* = \infty$, (b) $\rho_0^* = 60$ mm, and (c) $\rho_0^* = 30$ mm.

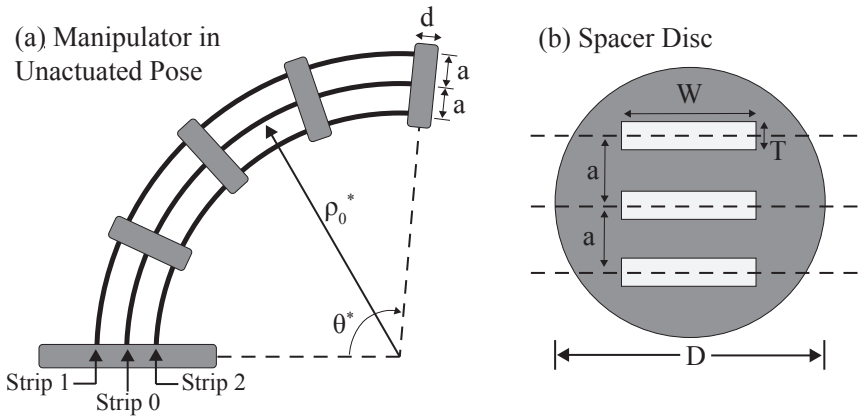

Figure 4: Definition of design parameters for prototype manipulators. (a) depicts a side view of the manipulator in its unactuated shape, and (b) depicts one of the spacer discs.

Table 1: Summary of the dimensions in the prototypes, as defined in Figure 4. Experimental calibration of these dimensions is described in Section 5.

Variable	**Variable definition**	**Desired dimension**	**Calibrated dimension**
D	Spacer disc diameter	7.8 mm	–
d	Spacer disc thickness	1.57 mm	–
a	Distance between strips	2.5 mm	A: 2.93 mm B: 2.86 mm C: 2.92 mm
T	Strip thickness	0.292 mm	–
W	Strip width	1.52 mm	–
L_0	Length of strip 0	40 mm	A: 40.04 mm B: 41.45 mm C: 42.02 mm
$\rho_0^* = \frac{1}{\kappa_0^*}$	Radius of precurvature of strip 0	A: ∞ B: 60 mm C: 30 mm	B: 65 mm C: 32.25 mm

amount of electrical current through it for a short period of time. Resistive heating in the nitinol heats the material to the temperature required for it to "memorize" the shape of the jig.

We created one straight prototype (Prototype A), one with an intended precurvature radius of 60 mm (Prototype B), and one with an intended precurvature radius of 30 mm (Prototype C). These radius values refer to the precurvature of the central backbone strip, ρ_0^* (with the star superscript denoting dimensions in the unactuated shape). The precurvature radii of the two actuation strips, ρ_i^*, are given by

$$\rho_i^* = \rho_0^* + a_i \tag{1}$$

where a_i is the distance from strip 0 to the i^{th} strip with positive a_i for elements on the outside of the curve and negative a_i for elements on the inside of the curve, such that

$$a_i = \begin{cases} 0, & i = 0 \\ a, & i = 1 \\ -a, & i = 2 \end{cases}. \tag{2}$$

Similarly, the length of each strip within the manipulator prior to actuation, L_i^*, is given by

$$L_i^* = L_0 \left(1 + \frac{a_i}{\rho_0^*}\right). \tag{3}$$

This is to prevent the strips from deflecting each other out of their set precurvatures and producing strain when the manipulator is in its unactuated shape. Behind the plate defining the base of the manipulator, where the force sensors were attached to the strips in the experiments of Section 5, an additional 7 mm of each actuation strip was set into the same circular arc. This portion represents the maximum length of strip inserted into the manipulator in our experiments, and precurving this portion allows us to treat the precurvature of each strip as constant within the manipulator even as the strips are translated during bending.

4. KINEMATIC & STATIC MODELING

To aid in the eventual design of a precurved manipulator for a specific application, we develop the following modeling framework relating translation of the strips, resulting curvature, strain in the manipulator and applied actuation forces, for a device such as the ones described in Section 3. We begin with a kinematic model, relating the translation of the actuation strips to the resulting curvature. We then use a statics model based on Castigliano's theorem, to model the actuation forces required to achieve a given manipulator curvature.

4.1 Kinematics

First, we assume a circularly curved manipulator shape (an assumption frequently applied in continuum robot modeling[1]), which allows us to fully describe each pose by a single value (e.g. the curvature κ_0 of the manipulator's centerline). The geometric relationship defined in Equation 1 should remain true as the device is actuated outside of its original shape, such that $\rho_i = \rho_0 + a_i$ during actuation. In terms of curvature, this is:

$$\kappa_i = \frac{\kappa_0}{1 + a_i \kappa_0} \tag{4}$$

where κ_i is the curvature of the i^{th} strip. To also maintain Equation 3 outside of the unactuated pose, the translation of each actuation strip must be:

$$\Delta L_i = L a_i \left(\kappa_0 - \kappa_0^*\right) \tag{5}$$

where κ_0 is the curvature of strip 0 and κ_0^* is the precurvature of strip 0. Since $a_1 = -a_2$, we can define a single actuation variable q as:

$$q = \Delta L_1 = -\Delta L_2. \tag{6}$$

The resulting kinematic relationship between q and the modeled curvature, κ_0 is:

$$\kappa_0(q) = \frac{La\kappa_0^* + q}{La}. \tag{7}$$

4.2 Statics

Various statics models have been developed for continuum robots, including constant curvature models such as the model we propose here, as well as more complex models which can describe arbitrary spatial curves (see [3] for a review). The statics model we use is derived based on a classic bending beam model of strain. This allows us to compute the total strain energy stored in the deflected structure, then estimate the actuation forces in each element based on Castigliano's theorem, similar to the method used in [18].

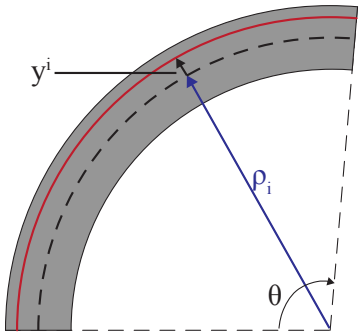

Figure 5: Definition of y^i, which describes the location of a fiber within the i^{th} strip relative to the centerline of the i^{th} strip.

We start by modeling the strain in a single precurved strip deflected to an arbitrary curvature. We assume pure bending, with the neutral bending plane of the element at its centerline.* The strain varies along y^i, the distance from the neutral plane of the bent elastic element to the location within that strip (illustrated in Figure 5). We can model strain as a function of y^i and κ_i according to:

$$\epsilon(y^i, \kappa_i) = \frac{y^i \left(\kappa_i - \kappa_i^*\right)}{1 + y^i \kappa_i^*}. \tag{8}$$

Next, we consider the stress in the material for a given strain value. The stress-strain relationship for nitinol at high strains is complex and nonlinear.[19,20] However, for the prototypes we constructed and the curvatures tested in Section 5, the strains can be considered to remain in a linear elastic region of the stress-strain curve, where

$$\sigma = E\epsilon. \tag{9}$$

Many other continuum manipulators made with nitinol operate in this linear elastic strain range.[4,11,21] For manipulators undergoing higher strains, models describing a larger portion of the stress-strain curve can be used. For example, a simple piecewise linear model which captures the plateau stress effects observed with nitinol is:

$$\sigma(\epsilon) = \begin{cases} \sigma_{lp}, & \epsilon < \frac{\sigma_{lp}}{E} \\ E\epsilon, & \frac{\sigma_{lp}}{E} \leq \epsilon \leq \frac{\sigma_{up}}{E} \\ \sigma_{up}, & \epsilon > \frac{\sigma_{up}}{E} \end{cases} \tag{10}$$

where σ_{up} is the upper plateau stress in tension and σ_{lp} is the lower plateau stress in compression. With a relationship between stress and strain defined, the strain energy density corresponding to any strain value can be computed by finding the area under the stress-strain curve:

$$w(\epsilon) = \int_0^{\epsilon} \sigma(u) du. \tag{11}$$

The total strain energy stored in each strip can then be found by integrating the strain energy density over the volume of the strip within the manipulator. In this integration, we neglect the strain energy stored in the precurved length of strip behind the front plate, which experiences some strain because it is straightened. Due to the short length in comparison to the total length of strip in the manipulator, we assume this transmission length will contribute relatively little to the strain energy. Additionally, since our two actuation strips are

*In general the neutral bending plane for a precurved beam is not at its geometric centerline, but defined by a curvature radius of $\rho_n = T\left(\ln\left(\frac{\rho_0+0.5T}{\rho_0-0.5T}\right)\right)^{-1}$. However, due to the very small thickness of the strips used in these prototypes, the difference between ρ_n predicted by this equation and the radius of the centerline is very slight (0.2% of the strip thickness even at the tightest curvature observed in our experiments).

always translated by equal and opposite amounts during actuation, the total length of precurved strip behind the front plate remains constant, and thus the amount of strain energy stored due to straightening in the transmission length will be approximately constant during actuation. With this simplifying assumption, the resulting expression for the strain energy in the i^{th} strip is found by integrating strain energy density over the strip's "reference" volume (in its unactuated shape):

$$U_i(\kappa_0) = \int_{V_i} w(\epsilon(\kappa_0, y^i))dV_i. \tag{12}$$

Summing the strain energy in each of the strips yields the total strain energy stored in the manipulator:

$$U(\kappa_0) = \sum_{i=0}^{2} U_i. \tag{13}$$

After finding the total strain energy, we can deduce the moment applied at the tip of the manipulator based on Castigliano's theorem, by considering the device as a single bending beam:

$$M(\kappa_0) = \frac{\partial U}{\partial \theta}, \tag{14}$$

where $\theta = L_0\kappa_0$ is the angle subtended by the arc of the manipulator. Based on a static balance at the tip disc, and assuming that the central strip sustains no tensile or compressive force since it is free to slide at the tip, we find that the actuation force in each of the two elements must be equal and opposite ($F_1 = -F_2 \triangleq F$).

The value of F, the tensile or compressive force sustained by each strip is found by:

$$F(\kappa_0) = \frac{M}{2a}, \tag{15}$$

where F represents tension on the strip which has been retracted (i.e. $\Delta L_i < 0$) and compression on the strip which has been inserted (i.e. $\Delta L_i > 0$).

5. EXPERIMENTS

To investigate the accuracy of the model described in Section 4, we attached each of our prototypes to a pair of linear positioning slides, as shown in Figure 6. The setup was assembled primarily from laser cut acrylic, with the same low-friction material which composes the spacer discs (PTFE-filled Delrin acetal resin) used for the front plate, where the strips are inserted and retracted from the manipulator. The total transmission length of each strip was kept to a minimum (11 mm) in order to minimize buckling. The back end of each of the actuation strips is attached to an acrylic piece with J-B Weld epoxy, which is mounted to a small six-axis force/torque sensor (Nano17, ATI Industrial Automation, USA) used to record the actuation forces on each strip.

Each prototype manipulator was mounted to the setup, and sequentially positioned with q values first increasing from 0 mm to 7 mm in increments of 1 mm, then decreasing from 0 mm to -7 mm in increments of 1 mm. For each pose tested, the actuation forces for each strip were recorded using the Nano17 sensors, and a photo of the manipulator pose was recorded. We considered the actuation force for each pose to be the norm of the three-dimensional force vector recorded by each sensor, averaged between the two sensors. The curvature of the pose was determined using the photos, by first recording 20 points along the central backbone strip using the image analysis program ImageJ, with the diameter of one of the spacer discs serving as a reference for size. These points were fit to a circle, whose radius defines the experimentally observed curvature radius of the manipulator.

To account for uncertainty in the prototype dimensions, we optimized the values of a and L_0 for each prototype and κ_0^* for each precurved prototype so as to reduce the error between the kinematic model and the experimentally observed curvatures. For the optimization, we assumed some reasonable bounds on the parameter values. For a, we allowed for optimization within ± 0.5 mm of the intended distance, which is reasonable given some oversizing of the slots in the discs. For the length L_0 and the radius of precurvature ρ_0^*, we used bounds at ± 3 mm and ± 5 mm from the intended values, respectively, which are also reasonable given imprecision in

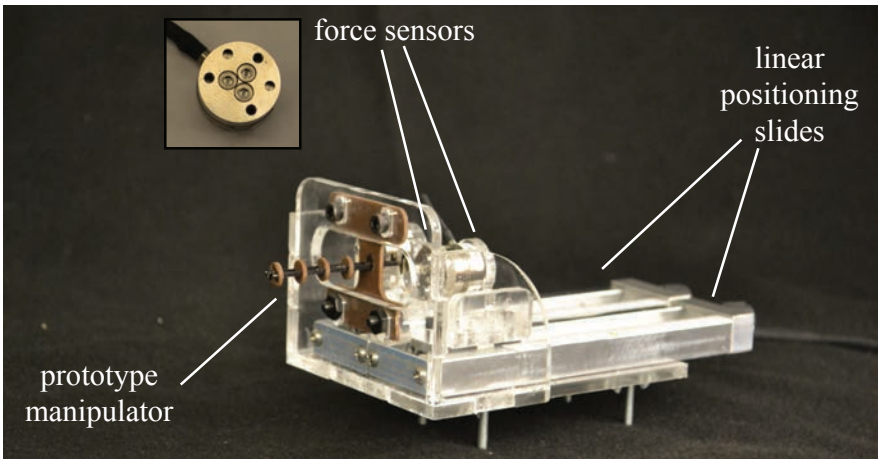

Figure 6: Experimental setup used to measure actuation forces.

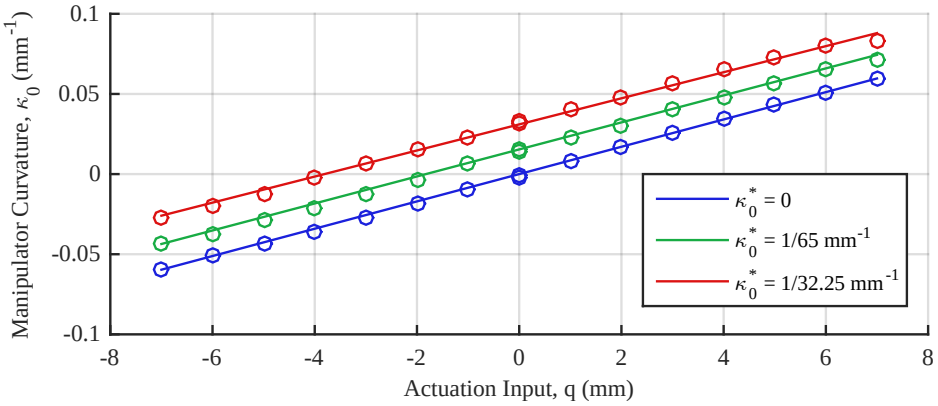

Figure 7: Kinematic model accuracy: experimentally observed curvature (open circles) and curvature predicted by the kinematic model (solid line) versus actuation input q.

the device assembly. The calibrated values for these variables are given in the last column of Table 1. With this calibration, the accuracy of the kinematic model is shown in Figure 7.

The experimentally observed force data was then used to fit the value of Young's modulus in the statics model so as to minimize the error between the observed and modeled actuation forces. The statics model is computed based on the modeled curvature, using the values for a, L_0 and κ_0^* which were calibrated previously. This resulted in a Young's modulus value of 59 GPa, which falls within the 41-75 GPa range reported in the manufacturer data sheet (Nitinol Devices and Components, Inc., USA). The observed and modeled forces plotted against curvature are shown in Figure 8. The result is a reasonable fit between the statics model and the experimental data, with unmodeled friction, imprecision in assembly of the prototypes, and changes in material property due to heat treatment being the most likely sources of error. Based on the experimental force data shown in Figure 8, if we assume an arbitrary actuation force limit of 5 N, the workspace of the straight and precurved manipulators is demonstrated in Figure 9.

6. CONCLUSIONS

We expect that the concepts described in this paper will become increasingly valuable when (1) high stiffness is required in the device and/or (2) the device is miniaturized to smaller diameters. One may want high stiffness in a variety of applications, such as when the continuum device is used as a retractor, for example. Smaller size is desirable in a variety of applications as well. One potential application might be endoscopic kidney stone

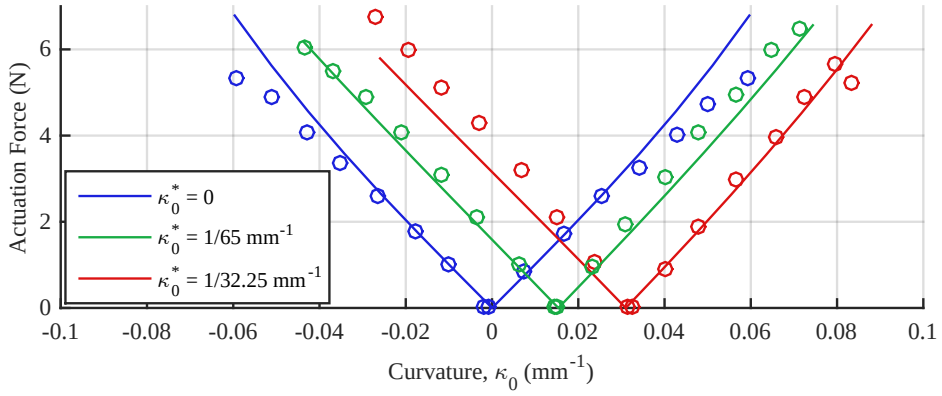

Figure 8: Statics model accuracy: experimentally observed actuation force versus observed curvature (open circles) and force predicted by the statics model versus curvature predicted by the kinematic model (solid line).

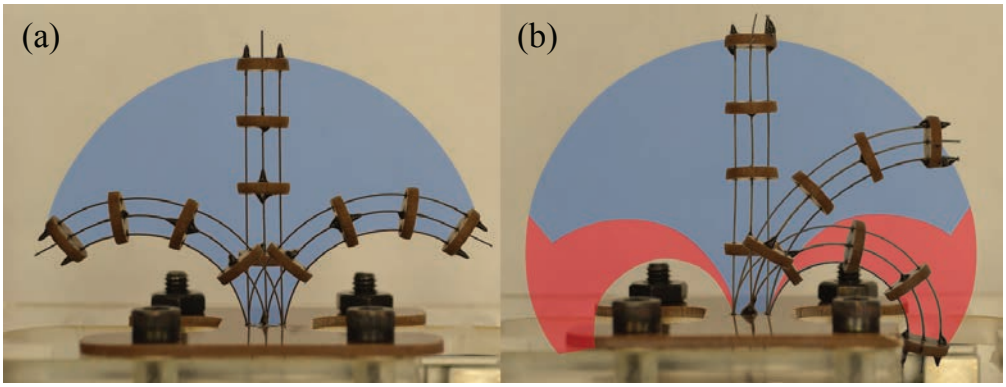

Figure 9: Comparison of the workspace of two prototypes subject to a 5 N limit on actuator force, based on the experimentally observed force data. (a) shows prototype A (no precurvature), and (b) shows prototype C (precurvature radius of approximately 30 mm). The red shaded region represents the expanded workspace of the precurved manipulator over that of the straight manipulator assuming axial rotation is possible.

treatment, where the ureteroscope used to access the stones may be approximately 2.5 mm in diameter. Increasing stiffness can be accomplished by increasing the dimensions of the elastic elements used in the manipulator. As can be seen from the model in Section 4, doing this increases the stored strain energy, and therefore requires larger actuation forces. Reducing the diameter of the device also increases actuation forces because it requires decreasing the spacing of the elastic elements, resulting in a smaller moment arm in Equation 15. Since the manipulator will have some maximum actuation force at which a component (for example, a glue bond or a support disc) risks failure, curvature will be limited by high actuation forces. Thus, the incorporation of precurvature will become increasingly valuable for smaller robots and for stiffer robots.

In summary, in this paper we have proposed the idea of using precurved elastic elements to "bias" the workspace of a continuum robot. This approach enables the device to reach around tighter corners than it would otherwise be able to, and when combined with axial rotation of the entire device, enables a larger workspace. We identified and briefly described two clinical applications that might benefit from higher curvature devices, namely hip revision surgery and endoscopic procedures requiring retroflexion, such as colonoscopy. We believe there will be many additional applications that can benefit from this approach as well. The model in this paper is primarily intended as a design tool, which will be useful for adapting the concept to specific clinical applications in the future.

REFERENCES

[1] Webster III, R. J. and Jones, B. A., "Design and kinematic modeling of constant curvature continuum robots: A review," *The International Journal of Robotics Research* **29**(13), 1661–1683 (2010).

[2] Robinson, G. and Davies, J. B. C., "Continuum robots – a state of the art," *IEEE International Conference on Robotics and Automation* **4**, 2849–2854 (1999).

[3] Burgner-Kahrs, J., Rucker, D. C., and Choset, H., "Continuum robots for medical applications: A survey," *IEEE Transactions on Robotics* **31**(6), 1261–1280 (2015).

[4] Camarillo, D. B., Milne, C. F., Carlson, C. R., Zinn, M. R., and Salisbury, J. K., "Mechanics modeling of tendon-driven continuum manipulators," *IEEE Transactions on Robotics* **24**(6), 1262–1273 (2008).

[5] Rucker, D. C. and Webster III, R. J., "Statics and dynamics of continuum robots with general tendon routing and external loading," *IEEE Transactions on Robotics* **27**(6), 1033–1044 (2011).

[6] Kutzer, M. D., Segreti, S. M., Brown, C. Y., Armand, M., Taylor, R. H., and Mears, S. C., "Design of a new cable-driven manipulator with a large open lumen: Preliminary applications in the minimally-invasive removal of osteolysis," *IEEE International Conference on Robotics and Automation* , 2913–2920 (2011).

[7] Degani, A., Choset, H., Zubiate, B., Ota, T., and Zenati, M., "Highly articulated robotic probe for minimally invasive surgery," *International Conference of the IEEE Engineering in Medicine and Biology Society* , 3273–3276 (2008).

[8] Simaan, N., Xu, K., Wei, W., Kapoor, A., Kazanzides, P., Taylor, R., and Flint, P., "Design and integration of a telerobotic system for minimally invasive surgery of the throat," *The International Journal of Robotics Research* **28**(9), 1134–1153 (2009).

[9] Simaan, N., "Snake-like units using flexible backbones and actuation redundancy for enhanced miniaturization," *IEEE International Conference on Robotics and Automation* , 3012–3017 (2005).

[10] Dupont, P. E., Lock, J., Itkowitz, B., and Butler, E., "Design and control of concentric-tube robots," *IEEE Transactions on Robotics* **26**(2), 209–225 (2010).

[11] Rucker, D. C., Jones, B. A., and Webster III, R. J., "A geometrically exact model for externally loaded concentric-tube continuum robots," *IEEE Transactions on Robotics* **26**(5), 769–780 (2010).

[12] Burgner, J., Swaney, P. J., Rucker, D. C., Gilbert, H. B., Nill, S. T., Russell III, P. T., Weaver, K. D., and Webster III, R. J., "A bimanual teleoperated system for endonasal skull base surgery," *IEEE/RSJ International Conference on Intelligent Robots and Systems* , 2517–2523 (2011).

[13] Hendrick, R. J., Herrell, S. D., and Webster III, R. J., "A multi-arm hand-held robotic system for transurethral laser prostate surgery," *IEEE International Conference on Robotics and Automation* , 2850–2855 (2014).

[14] Duerig, T., Pelton, A., and Stöckel, D., "An overview of nitinol medical applications," *Materials Science and Engineering: A* **273**, 149–160 (1999).

[15] Hanson, J., Atkin, W., Cunliffe, W., Browell, D., Griffith, C., Varma, J., and Plusa, S., "Rectal retroflexion: an essential part of lower gastrointestinal endoscopic examination," *Diseases of the Colon & Rectum* **44**(11), 1706–1708 (2001).

[16] Esber, E. and Yang, P., "Retroflexion of the sigmoidoscope for the detection of rectal cancer.," *American Family Physician* **51**(7), 1709–1711 (1995).

[17] Gilbert, H. B. and Webster III, R. J., "Rapid, reliable shape setting of superelastic nitinol for prototyping robots," *IEEE Robotics and Automation Letters (In Press)* (2016).

[18] York, P. A., Swaney, P. J., Gilbert, H. B., and Webster III, R. J., "A wrist for needle-sized surgical robots," *IEEE International Conference on Robotics and Automation* , 1776–1781 (2015).

[19] Pelton, A. R., Dicello, J., and Miyazaki, S., "Optimisation of processing and properties of medical grade nitinol wire," *Minimally Invasive Therapy & Allied Technologies* **9**(2), 107–118 (2000).

[20] Reedlunn, B., Churchill, C. B., Nelson, E. E., Shaw, J. A., and Daly, S. H., "Tension, compression, and bending of superelastic shape memory alloy tubes," *Journal of the Mechanics and Physics of Solids* **63**, 506–537 (2014).

[21] Jones, B. A., Gray, R. L., and Turlapati, K., "Three dimensional statics for continuum robotics," *IEEE/RSJ International Conference on Intelligent Robots and Systems* , 2659–2664 (2009).